Combined Cloud Microphysics Data Set for ORACLES

Joseph O'Brien[1], Siddhant Gupta[2], Greg McFarquhar[2], Michael Poellot[1], David Delene[1], and Jennifer Griswold[3]

[1]University of North Dakota, [2]University of Oklahoma, [3]University of Hawaii

Principal Investigators (PIs): Greg McFarquhar (mcfarq@ou.edu) and Michael Poellot (michael.poellot@und.edu)

Phase Doppler Interferometer (PDI) PI: Jennifer Griswold (smalljen@hawaii.edu)

Group members: Joseph O'Brien (joseph.r.obrien@und.edu), Siddhant Gupta (sid@ou.edu), and David Delene (david.delene.und@gmail.com)

1. Introduction

This is a derived data set of cloud microphysical and state parameters obtained using in-situ cloud probes during the NASA ObseRvations of Aerosols above CLouds and their intEractionS (ORACLES) field campaign (Gupta et al., 2021a,b; Redemann et al., 2021). The data were derived from files uploaded to the NASA ESPO archive (ORACLES Science Team, 2020a-c). State variables (temperature, pressure, and dew point temperature) were retrieved from 1-Hz merged data files compiled by Yohei Shinozuka. The latest revisions of merged files from ORACLES 2016, 2017, and 2018 were used (R36, R28, and R25, respectively.)

The PDI data were provided by the instrument PI. Other cloud probe data were processed and uploaded to the archive by Joseph O'Brien as "UND-[probe]". Data from the 2-Dimensional Stereo Probe (2D-S) and the High Volume Precipitation Sampler (HVPS-3) were processed by Siddhant Gupta using the University of Illinois/Oklahoma Optical Array Probe Processing Software (McFarquhar et al., 2018) and uploaded to the archive as "OU-[probe]". The NASA ESPO archive also contains 2D-S and HVPS-3 data processed by Joseph O'Brien using the System for OAP Data Analysis (SODA). The microphysics data files use the UIOOPS size distributions, $N(D)$, in terms of droplet diameter D at 1 second resolution. The $N(D)$ was used to calculate the total number concentration N, effective radius re, liquid water content LWC, rain rate R, radar reflectivity factor Z, extinction of liquid drops β, and mean volume radius rv (Table 1).

Queries about the data should be directed to the respective instrument PIs and collaboration with the group on the use of these data is strongly encouraged since different applications may benefit from different processing methodologies. There are caveats associated with the use of these data which are difficult to thoroughly document. Each file is in the netCDF

format and named 'Microphysics_P3_YYMMDD_R0.nc' where YYMMDD corresponds to the year, month, and date for the research flight (Table 2). R0 indicates the file version/revision number (starting with 0). Each file contains the following variables in units specified within parenthesis and dimensions specified within square brackets. Parameters listed below in bold fonts were retrieved directly from the files already uploaded to the NASA ESPO archive, while non-bold font parameters are derived variables unique to this data set.

Dimensions:

'time': timestamp for each 1-Hz data sample

'bins': number of size bins for the merged droplet size distribution from multiple probes

Parameters:

'time': UTC Time ("HHMMSS") [time, 6]

'timevec': Time in days since Jan 0 0000 (MATLAB date format) [time, 1]

'altitude': Aircraft altitude (meters above mean sea level) [time, 1]

'latitude': Aircraft latitude (˚ N) [time, 1]

'longitude': Aircraft longitude (˚ E) [time, 1]

'temp': Static Air Temperature (˚C) [time, 1]

'temp_d': Dew Point Temperature (˚C) [time, 1]

'pres': Static Pressure (mb) [time, 1]

'King LWC': Bulk liquid water content from the King hot-wire (g m^{-3}) [time, 1]

'bin_min': Lower end of size bins (*D*) used for the merged droplet size distribution from multiple probes (µm) [bins, 1]

'bin_max': Upper end of size bins (*D*) used for the merged droplet size distribution from multiple probes (µm) [bins, 1]

'bin_mid': Midpoint of size bins (*D*) used for the merged droplet size distribution from multiple probes (µm) [bins, 1]

'Nd': Number concentration of drops in a given bin, not normalized (cm^{-3}) [time, bins]

'N': Total droplet concentration (integrated over bin sizes with $D > 3$ μm) (cm^{-3}) [time, 1]

'Nc': Cloud droplet concentration (integrated over $3 < D < 50$ μm) (cm^{-3})   [time, 1]

'Nc50': Drizzle drop concentration (integrated over $D > 50$ μm) (cm^{-3})   [time, 1]

're': Effective radius of liquid drops (μm)   [time, 1]

'CWC': Cloud Water Content (liquid water content for $D < 50$ μm) (g m^{-3})   [time, 1]

'RWC': Rainwater Content (liquid water content for $D > 50$ μm) (g m^{-3})   [time, 1]

'LWC': Liquid water content from the entire size distribution (g m^{-3})   [time, 1]

'R': Rain rate (calculated using the droplet mass and fall speeds for drizzle drops ($D > 50$ μm) (mm h^{-1})   [time, 1]

'Na': Accumulation-mode ($0.1 < D < 3$ μm) aerosol concentration from the PCASP outside cloud (cm^{-3})   [time, 1]

'Z': Radar reflectivity factor (dBZ)   [time, 1]

'beta': Extinction of liquid drops (km^{-1})   [time, 1]

'rv': Mean volume radius of liquid drops (μm)   [time, 1]

2. Instrumentation

ORACLES had three Intensive Observation Periods (IOPs) based at Walvis Bay, Namibia in September 2016, and based at Sao Tome and Principe in August 2017 and October 2018. The NASA P-3B aircraft was equipped with in-situ cloud probes whose data were used to calculate cloud properties (Table 3). The cloud probes included a PDI (Chuang et al., 2008), a Cloud and Aerosol Spectrometer (CAS) on the Cloud, Aerosol and Precipitation Spectrometer (CAPS) (Baumgardner et al., 2001), a 2D-S (Lawson et al., 2006), and an HVPS-3 (Lawson et al., 1998). A single Cloud Droplet Probe CDP (Lance et al., 2010) was used during the 2016 IOP (CDP-A). A second CDP (CDP-B) was added for the 2017 and 2018 IOPs. CDP-A was replaced by a third CDP (CDP-C) for the 2018 IOP. These instruments sampled $N(D)$ for droplets with D from 0.5 μm to 19200 μm. A King hot-wire was used to sample bulk LWC (King et al., 1978). The Passive Cavity Aerosol Spectrometer Probe (PCASP) measured accumulation-mode aerosol $N(D)$ from 0.1 to 3.0 μm to calculate N_a (Cai et al., 2013).

The probes were calibrated by the manufacturers before and after the IOPs. Performance checks were completed during the IOPs following the instrument manuals to monitor instrument performance. This included monitoring the probe voltages and temperatures during flights and

passing calibration particles through the CAS/CDP sample volume to determine changes in the relationship between particle size and peak signal voltage. Before each flight, optical lenses of the probes were cleaned with isopropyl. Nevertheless, soot deposition occurred on the lenses during flight legs through dense aerosol plumes.

The "OU-2DS" and "OU-HVPS3" files were used for creating this dataset. The remaining data (except PDI) were processed using the Airborne Data Processing and Analysis processing package (Delene, 2011). The following procedures were followed for processing the 2D-S and HVPS-3 data. "Droplets measured by the 2D-S or HVPS-3 with aspect ratios greater than 4 or area ratios less than 0.5 were rejected as artifacts. Droplets with inter-arrival times less than 6 µs, indicative of intermittently stuck diodes or drizzle breakup, were removed (Field et al., 2006). Out-of-focus hollow particles were reconstructed following Korolev (2007)" (Gupta et al., 2021a).

Data files were not created for aborted flights or flights when instrument issues meant that $N(D)$ of high quality was not available (Table 4). CAS data were unusable before 6 September 2016 (and after 7 October 2018) because of electronics issues. PDI data were unusable for ORACLES 2017 and 2018 due to electrical interference which affected data transfer between the instrument and onboard computers. CDP-A data were unusable for ORACLES 2016 and 2017 due to an optical misalignment issue. Nevertheless, more than one independent measurement of $N(D)$ was made for droplets with $D < 50$ µm during each flight (Table 2).

Differences between droplet measurements within overlap regions from different probes were examined to select the best estimate of $N(D)$ (Gupta et al., 2021b). The differences between N_c and LWC from the probes were determined and their statistical significance was tested using a two-sample t-test. The full spectrum of $N(D)$ was determined by merging the size distributions from multiple probes. Only droplets with $D > 3$ µm were considered to avoid the impact of aerosols in the droplet size distributions. CAS data were used to create the merged $N(D)$ for ORACLES 2016, CAS/CDP-B data for ORACLES 2017, and CDP-B/CDP-C data for ORACLES 2018 (Table 2). $N(D)$ from the CAS/CDP-B/CDP-C was merged with that of the 2D-S horizontal channel with a cross-over at $D = 50$ µm, and that of HVPS-3 with a cross-over at $D = 1050$ µm.

3. Cloud Probe Data Comparisons

a. 2016 IOP - CAS versus PDI

For ORACLES 2016, CAS and PDI $N(D)$ were available for droplets with $D < 50$ µm (Table 2). N_c and LWC were calculated for 16,559 1-Hz in-cloud data samples using the CAS and PDI droplet size distributions. In-cloud data samples were defined by $N_c > 10$ cm^{-3} as measured by the CAS and PDI, and LWC > 0.05 g m^{-3} as measured by the King hot-wire. CAS and PDI data were compared for nine research flights between 6 and 27 September 2016 when both instruments were operational. The average PDI N_c was 163.6 ± 90.3 cm^{-3} and the average CAS N_c was $153.0 \pm$

72.1 cm^{-3}, where the error estimates represent the standard deviation. The PDI N_c and CAS N_c were correlated with R_o = 0.88 (Fig. 1) but the average PDI N_c was significantly higher than the average CAS N_c (95% confidence intervals (CIs): 8.9 to 12.4 cm^{-3} higher).

The average PDI LWC was 0.35 ± 0.19 g m^{-3}, and the average CAS LWC was 0.15 ± 0.09 g m^{-3}. The LWC*s* were correlated with R_o = 0.84 but the average PDI LWC was significantly higher than the average CAS LWC (95% CIs: 0.19 to 0.20 cm^{-3} higher). The PDI LWC and CAS LWC were compared with the LWC measured by a King hot-wire (King LWC) which had an average value of 0.28 ± 0.15 g m^{-3} for the same data samples (Fig. 2). The average PDI LWC was significantly higher than the average King LWC (95% CIs: 0.06 to 0.07 g m^{-3} higher) while the average CAS LWC was significantly lower than the average King LWC (95% CIs: 0.13 to 0.14 g m^{-3} lower).

Vertical profiles of CAS LWC, PDI LWC, and King LWC were compared (Fig. 3) against the adiabatic LWC (hereafter LWC$_{ad}$) calculated for cloud profiles flown on six research flights from the 2016 IOP (PRFs 05, 07, 08, 09, 11, and 13). The average CAS LWC and King LWC were significantly lower than the average LWC$_{ad}$ (95% CIs: 0.16 to 0.17 g m^{-3} lower for CAS LWC and 0.01 to 0.03 g m^{-3} lower for King LWC). However, the average PDI LWC was significantly higher than the average LWC$_{ad}$ (95% CIs: 0.04 to 0.06 g m^{-3} higher). CAS data were used to create the best estimate files for ORACLES 2016 since the PDI LWC overestimated the bulk and LWC$_{ad}$. The use of King LWC is advised over CAS LWC due to better agreement between King LWC and LWC$_{ad}$.

b. 2017 IOP - CAS versus CDP-B

For ORACLES 2017, CAS and CDP-B $N(D)$ were available for droplets with D < 50 μm. N_c and LWC from CAS and CDP-B were compared for 13,251 1-Hz in-cloud samples collected during 12 research flights between 12 August and 2 September 2017 (Table 2). The average CDP-B N_c (192.3 ± 122.6 cm^{-3}) and CDP-B LWC (0.18 ± 0.16 g m^{-3}) were greater than the average CAS N_c (180.6 ± 96.5 cm^{-3}) and CAS LWC (0.09 ± 0.07 g m^{-3}). The average King LWC (0.21 ± 0.15 g m^{-3}) was significantly greater than the average CDP-B LWC (95% CIs: 0.02 to 0.02 g m^{-3} higher) and the average CAS LWC (95% CIs: 0.11 to 0.11 g m^{-3} higher).

For the research flights flown on 30 and 31 August 2017, the average CDP-B N_c (109.3 ± 39.5 cm^{-3}) and CDP-B LWC (0.05 ± 0.04 g m^{-3}) were 96 cm^{-3} and 0.16 g m^{-3} lower than the corresponding averages for other flights. In comparison, the average CAS N_c (145.79 ± 46.10 cm^{-3}) and CAS LWC (0.11 ± 0.05 g m^{-3}) for these two flights were 41 cm^{-3} lower and 0.02 g m^{-3} higher than the corresponding averages for other flights. The average King LWC for these flights (0.18 ± 0.10 g m^{-3}) was 0.03 g m^{-3} lower than the average King LWC for other flights. Since the relative changes in King LWC and CAS LWC compared to other flights were much smaller, it is unlikely the CDP-B LWC estimates from 30 and 31 August 2017 were accurate. Therefore, CAS data were used

to create best estimate files for 30 and 31 August 2017 (Table 2) and these flights are excluded from the comparisons below.

The N_c and LWC from CDP-B and CAS were compared for 11,438 1-Hz data samples from 10 research flights from the 2017 IOP (Table 2). The CDP-B more frequently sampled $N_c > 300$ cm^{-3} (2536 1-Hz samples) than the CAS (1623 1-Hz samples) and the average CDP-B N_c was significantly higher (95% CIs: 16.5 to 22.4 cm^{-3} higher) than the average CAS N_c (Fig. 4). The average CDP-B LWC was significantly higher (95% CIs: 0.11 to 0.12 g m^{-3} higher) than the average CAS LWC (Fig. 4). For 75% of the samples with CDP-B $N_c < 300$ cm^{-3}, CAS N_c and CDP-B N_c had minor differences (95% CIs: 0.84 to 5.39 cm^{-3}) but the average CDP-B LWC was still significantly higher than the average CAS LWC (95% CIs: 0.09 to 0.10 g m^{-3}) (Fig. 4).

The average King LWC (0.19 ± 0.13 g m^{-3}) was comparable to the average CDP-B LWC (0.18 ± 0.13 g m^{-3}) while the average CAS LWC (0.08 ± 0.06 g m^{-3}) was considerably lower than CDP-B LWC and King LWC (Fig. 5). The CAS LWC, CDP-B LWC, and King LWC were compared against LWC$_{ad}$ (Fig. 6) for cloud profiles flown on seven research flights from the 2017 IOP (PRFs 01, 02, 03, 04, 07, 08, and 10). The average LWC$_{ad}$ was significantly greater than each LWC but the differences with CAS LWC (95% CIs: 0.17 to 0.19 g m^{-3} higher) were much greater than those with CDP-B LWC (95% CIs: 0.05 to 0.07 g m^{-3} higher) and King LWC (95% CIs: 0.05 to 0.07 g m^{-3} higher). CDP-B data were used to characterize droplets with $3 < D < 50$ μm sampled during the 2017 IOP because CDP-B LWC had better agreement with King LWC and LWC$_{ad}$ compared to the CAS LWC.

c. 2018 IOP - CAS versus CDP-B

For the 2018 IOP, measurements from the CAS and CDP-B were compared for 5,518 1-Hz in-cloud samples from six research flights when the CAS was operational (Table 2). The average CDP-B N_c (124.8 ± 91.9 cm^{-3}) was significantly greater than the average CAS N_c (106.3 ± 66.9 cm^{-3}) (95% CIs: 15.5 to 21.5 cm^{-3} higher) (Fig. 7). The average CDP-B LWC (0.21 ± 0.14 g m^{-3}) had better agreement with the average King LWC (0.20 ± 0.12 g m^{-3}) compared to the average CAS LWC (0.10 ± 0.07 g m^{-3}) (Fig. 8). CAS LWC, CDP-B LWC, and King LWC were compared against LWC$_{ad}$ (Fig. 9). The average LWC$_{ad}$ was closer to the average CDP-B LWC (95% CIs: 0.04 to 0.06 g m^{-3} higher) and the average King LWC (95% CIs: 0.07 to 0.08 g m^{-3} higher) compared to the average CAS LWC (95% CI: 0.18 to 0.19 g m^{-3} higher). It was hypothesized that CDP-B provided better estimates of droplets with $3 < D < 50$ μm compared to the CAS for the first six research flights from the 2018 IOP. Thus, CAS data were not used to create the best estimate files.

d. 2018 IOP - CDP-B versus CDP-C

For ORACLES 2016, all cloud probes were installed on newly designed pylons that placed the cloud probes directly underneath the wing rather than slightly ahead of its leading edge, as commonly regarded as best practice. Consequently, there was concern that air flow into a probe

sample volume could have been affected by airflow perturbations induced by the wing, potentially affecting the measurement of $N(D)$ and calculation of N_c. To investigate this, a new pylon was used during ORACLES 2017 and 2018 which placed the CAS and CDP-B slightly lower and ahead of the leading edge of the aircraft wing, compared to other probes.

CDP-B and CDP-C had different mounting locations relative to the aircraft wing due to the use of a new pylon for CDP-B. The mounting locations of CDP-B and CDP-C were switched after 10 October 2018 to isolate the impact of instrument differences from the influence of the mounting location on the *CDP* measurements. Therefore, CDP data are compared for flights up to 10 October and for flights after 10 October separately. During the post-campaign instrument evaluation, it was found that the CDPs recorded similar counts for D > 7.5 μm but CDP-B recorded higher droplet counts for $D < 7.5$ μm compared to CDP-C (O'Brien et al., 2019; O'Brien et al., 2021, in prep). To minimize instrument-related differences, N_c^* and LWC* were calculated using $N(D > 7.5)$ and compared along with N_c and LWC.

For the seven flights up to 10 October, the differences between the average CDP-B and CDP-C N_c were statistically insignificant but CDP-C N_c^* was up to 12.6 cm⁻³ higher than CDP-B N_c^*, on average (Fig. 10). The average CDP-C LWC was up to 0.02 g m⁻³ higher than CDP-B LWC with similar differences between the two LWC* (Fig. 11). On average, the CDP-B LWC and CDP-C LWC were up to 0.01 and 0.03 g m⁻³ higher than the bulk LWC (Fig. 12). Due to close agreement between the two *CDP* LWC and bulk LWC, it is unlikely the use of either *CDP* would significantly impact data quality. Data from CDP-B (mounted on the new pylon alongside the CAS for these flights) were used to create the data files to maintain consistency between 2017 and 2018 data.

For flights after 10 October, CDP-C was mounted on the new pylon alongside the CAS. On 15 October, an issue with CDP-C qualifier voltages led to anomalously high CDP-C N_c (not shown). Therefore, data from CDP-B were used for the data file for 15 October. For the remaining five flights, the average CDP-B N_c was up to 30.9 cm⁻³ higher than CDP-C N_c. These differences were partly driven by droplet counts for D < 7.5 μm and the average CDP-B N_c* was only up to 11 cm⁻³ greater than CDP-C N_c* (Fig. 13). On average, the CDP-B LWC was up to 0.03 g m⁻³ higher than the CDP-C LWC with similar differences between the LWC* measurements (Fig. 14). Data from CDP-C were used to create the data files for these five flights because the high CDP-B N_c (> 500 cm⁻³) were likely an artifact due to the overestimation of $N(D < 7.5)$ compared to CDP-C (Fig. 13).

e. **2017 and 2018 IOPs - 2D-S horizontal and vertical channel**

The 2D-S is a stereo probe with a horizontal and vertical channel which concurrently sampled the cloud volume. Data from the vertical channel were unusable for ORACLES 2016 due to soot deposition on the optical lenses. Therefore, data from the horizontal channel were used to characterize $N(D)$ for D > 50 μm for ORACLES 2016. During ORACLES 2017 and 2018, N_c and

LWC sampled by both horizontal (N_H and LWC$_H$) and vertical (N_V and LWC$_V$) channels. N_H and N_V were strongly correlated for both IOPs (Fig. 15) with similarly high correlations between LWC$_H$ and LWC$_V$ (Fig. 16). To maintain consistency, data from the horizontal channel were used for all deployments despite the availability of data from the vertical channel for ORACLES 2017 and 2018. However, this is unlikely to impact data quality since these data were highly correlated.

Table 1: List of parameters included in the microphysics data files

Parameters	
Size distribution, N(D)	CAS/CDP-B/CDP-C: $N(3 < D < 50 \text{ μm})$ 2DS: $N(50 < D < 1300 \text{ μm})$ HVPS-3: $N(D > 1300 \text{ μm})$
Bulk Liquid Water Content, LWC	King hot-wire
Droplet concentration, N_c	$\displaystyle\sum_{D_{min}}^{D_{max}} N(D)$
Effective radius, re	$\dfrac{\sum_{D=D_{min}}^{D_{max}} N(D)D^3}{2 \sum_{D=D_{min}}^{D_{max}} N(D)D^2}$
LWC	$\displaystyle\sum_{D=D_{min}}^{D_{max}} N(D)\frac{\pi}{6}D^3$
Rain rate, R u(D) from Rogers (1976)	$\displaystyle\sum_{50 \text{ μm}}^{D_{max}} u(D)\, N(D)\frac{\pi}{6}D^3$ $u(D) = 1.19 \times 10^6 \,(D/2)^2 \;[D < 40 \text{ μm}]$ $= 8 \times 10^3 \,(D/2)^2 \;[40 < D < 600 \text{ μm}]$ $= 2.01 \times 10^3 \,(D/2)^2 \;[D > 600 \text{ μm}]$
Radar reflectivity factor, Z	$\displaystyle\sum_{D_{min}}^{D_{max}} N(D)D^6$
Total extinction, β	$\displaystyle\sum_{D=D_{min}}^{D_{max}} 2\, N(D)\frac{\pi}{4}D^2$

Table 2: List of P-3 research flights (PRFs) when microphysics data files were created. Instruments that sampled droplets with 3 < D < 50 μm are listed (instrument with best estimate of N(D) used to create data files is in bold). Adapted from Gupta et al. (2021b).

PRF number and date	Instruments
PRF05Y16: Sep. 06	**CAS**, PDI
PRF06Y16: Sep. 08	**CAS,** PDI
PRF07Y16: Sep. 10	**CAS**, PDI
PRF08Y16: Sep. 12	**CAS**, PDI
PRF09Y16: Sep. 14	**CAS**, PDI
PRF10Y16: Sep. 18	**CAS**, PDI
PRF11Y16: Sep. 20	**CAS**, PDI
PRF13Y16: Sep. 25	**CAS**, PDI
PRF01Y17: Aug. 12	CAS, **CDP-B**
PRF02Y17: Aug. 13	CAS, **CDP-B**
PRF03Y17: Aug. 15	CAS, **CDP-B**
PRF04Y17: Aug. 17	CAS, **CDP-B**
PRF05Y17: Aug. 18	CAS, **CDP-B**
PRF07Y17: Aug. 21	CAS, **CDP-B**
PRF08Y17: Aug. 24	CAS, **CDP-B**
PRF09Y17: Aug. 26	CAS, **CDP-B**
PRF10Y17: Aug. 28	CAS, **CDP-B**
PRF11Y17: Aug. 30	**CAS**, CDP-B
PRF12Y17: Aug. 31	**CAS**, CDP-B
PRF13Y17: Sep. 02	CAS, **CDP-B**
PRF01Y18: Sep. 27	CAS, **CDP-B**, CDP-C
PRF02Y18: Sep. 30	CAS, **CDP-B**, CDP-C
PRF03Y18: Oct. 02	CAS, **CDP-B**, CDP-C
PRF04Y18: Oct. 03	CAS, **CDP-B**, CDP-C
PRF05Y18: Oct. 05	CAS, **CDP-B**, CDP-C
PRF06Y18: Oct. 07	CAS, **CDP-B**, CDP-C
PRF07Y18: Oct. 10	**CDP-B**, CDP-C
PRF08Y18: Oct. 12	CDP-B, **CDP-C**
PRF09Y18: Oct. 15	**CDP-B**, CDP-C
PRF10Y18: Oct. 17	CDP-B, **CDP-C**
PRF11Y18: Oct. 19	CDP-B, **CDP-C**
PRF12Y18: Oct. 21	CDP-B, **CDP-C**
PRF13Y18: Oct. 23	CDP-B, **CDP-C**

Table 3: Main parameter used, sampling frequency, measurement range for instruments used. Adapted from Gupta et al. (2021a).

Instrument	Parameter used	Sampling Frequency	Measurement Range	Reference
Rosemount 102	Temperature	1 Hz	Nominally -50° to 50°C	Rosemount, Incorporated
Rosemount MADT 2014	Pressure	1 Hz	Nominally 30 - 1300 mb	Rosemount, Incorporated
EdgeTech 137 Chilled-Mirror Hygrometer	Dew Point Temperature	1 Hz	Nominally -40° to 60°C	EdgeTech Instruments
Global Positioning System	Latitude, Longitude, Altitude	1 Hz	-90 to 90° -180 to 180°	
CAS	Droplet n(D)	10 Hz	0.5 - 50 µm	Baumgardner et al. (2001)
CDP	Droplet n(D)	10 Hz	2 – 50 µm	Lance et al. (2010)
2D-S	Droplet Images, asynchronous n(D)		Nominally 10 - 1,280 µm	Lawson et al. (2006)
HVPS-3	Droplet Images, asynchronous n(D)		Nominally 150 - 19,200 µm	Lawson et al. (1998)
King Hot-wire	Bulk LWC	25 Hz	0.05 - 3 g m^{-3}	King et al. (1978)
PCASP	Aerosol n(D)	10 Hz	0.1 - 3 µm	Strapp et al. (1992)

Table 4: List of P-3 research flights (PRFs) when microphysics data files were not created because a best-estimate for N(D) over the entire droplet size range was not available.

PRF number and date	Notes
PRF01Y16: Aug. 30	Aborted flight
PRF02Y16: Aug. 31	CAS not working, poor quality N(D < 50 μm)
PRF03Y16: Sep. 02	CAS not working, poor quality N(D < 50 μm)
PRF04Y16: Sep. 04	CAS not working, poor quality N(D < 50 μm)
PRF12Y16: Sep. 24	poor quality N(D > 50 μm) from 2-DS
PRF06Y17: Aug. 19	Aborted flight
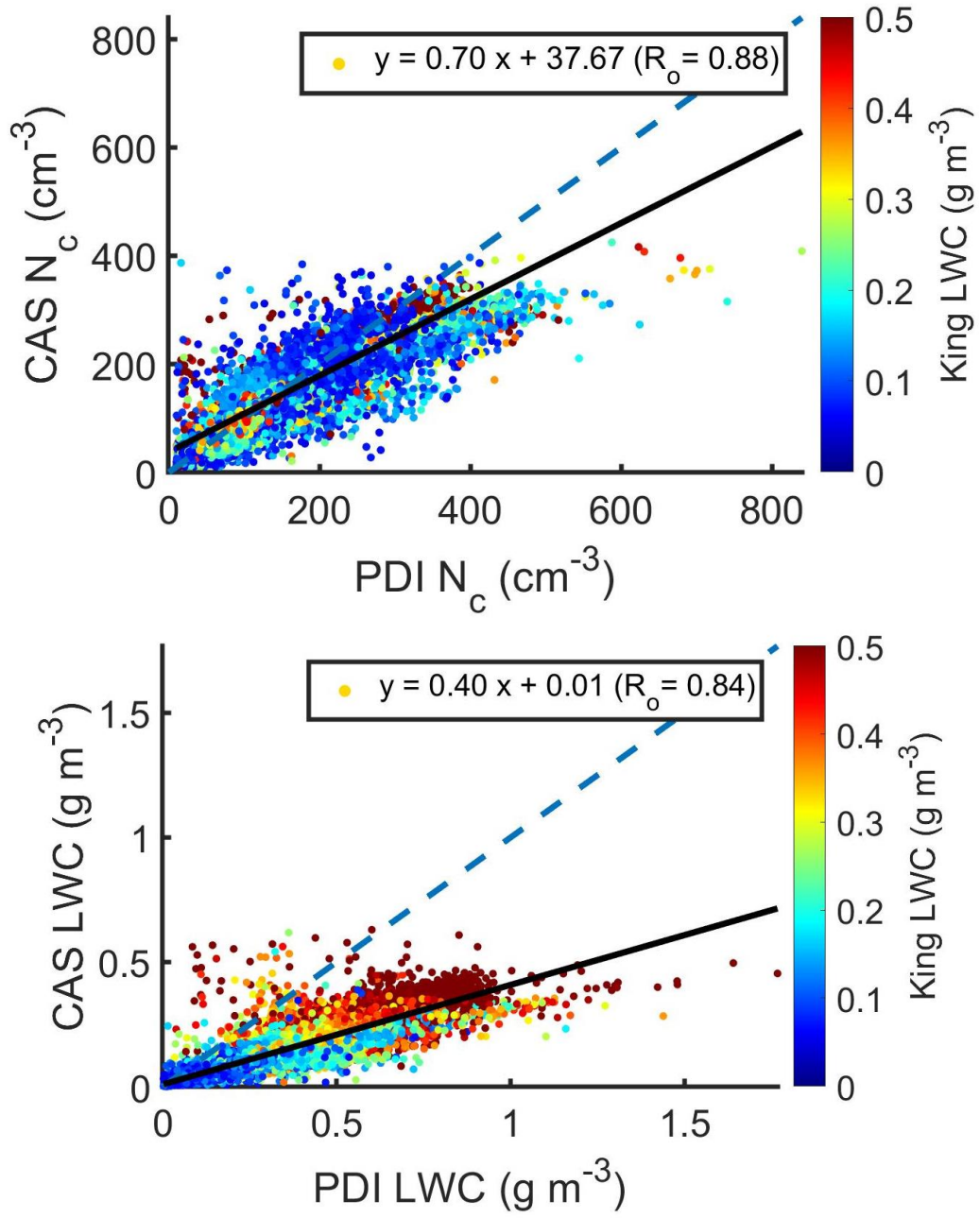
Figure 1: Scatter plots between N_c (top) and LWC (bottom) from CAS and PDI during nine research flights from ORACLES 2016. Each point represents a 1-Hz data sample colored by bulk LWC from the King hot-wire. Legend contains linear regression coefficients and Pearson's correlation coefficient (R_o).
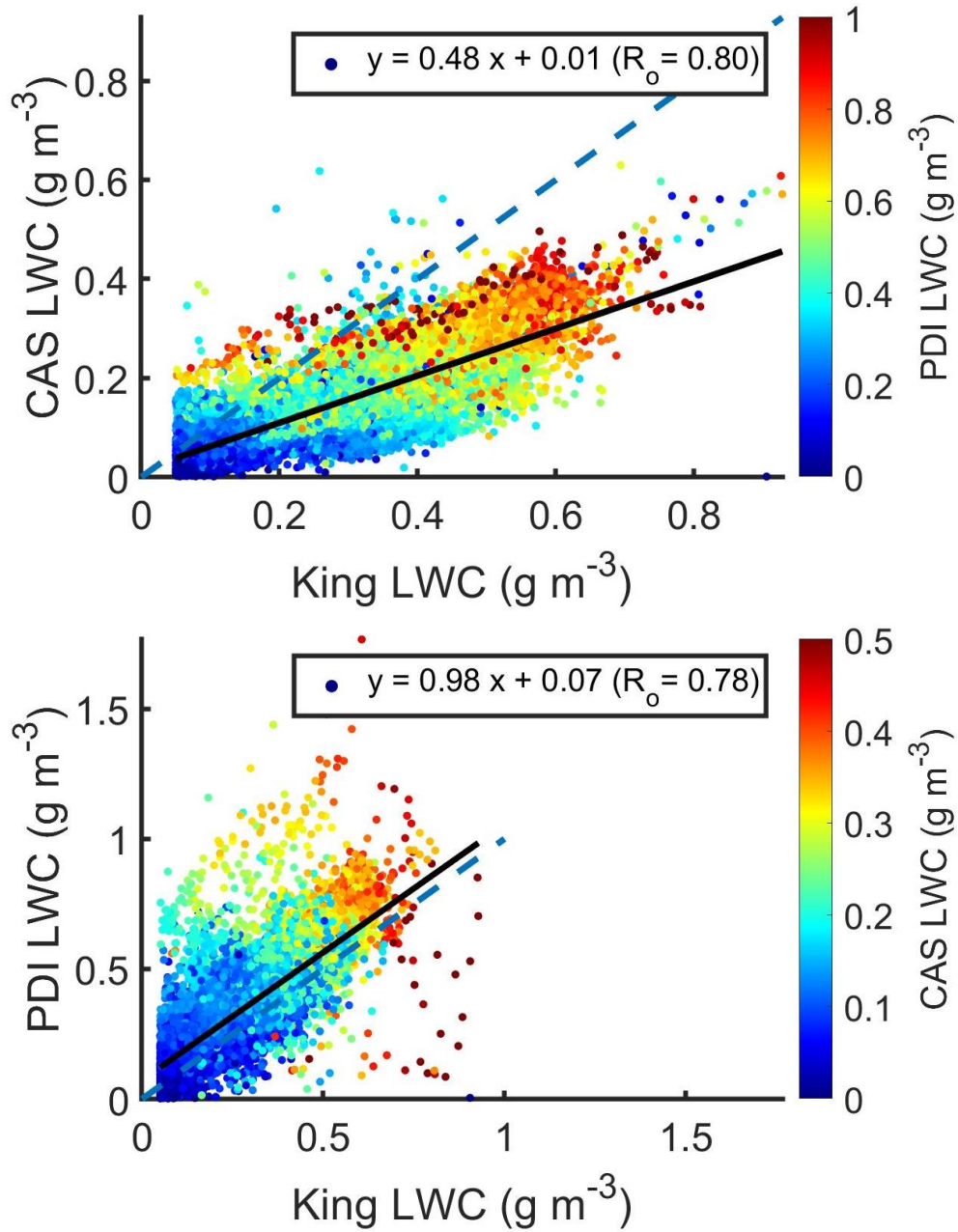
Figure 2: Scatter plots between bulk LWC with CAS LWC (top) and PDI LWC (bottom) for ORACLES 2016. Each point represents a 1-Hz data sample colored by PDI LWC (top) and CAS LWC (bottom).
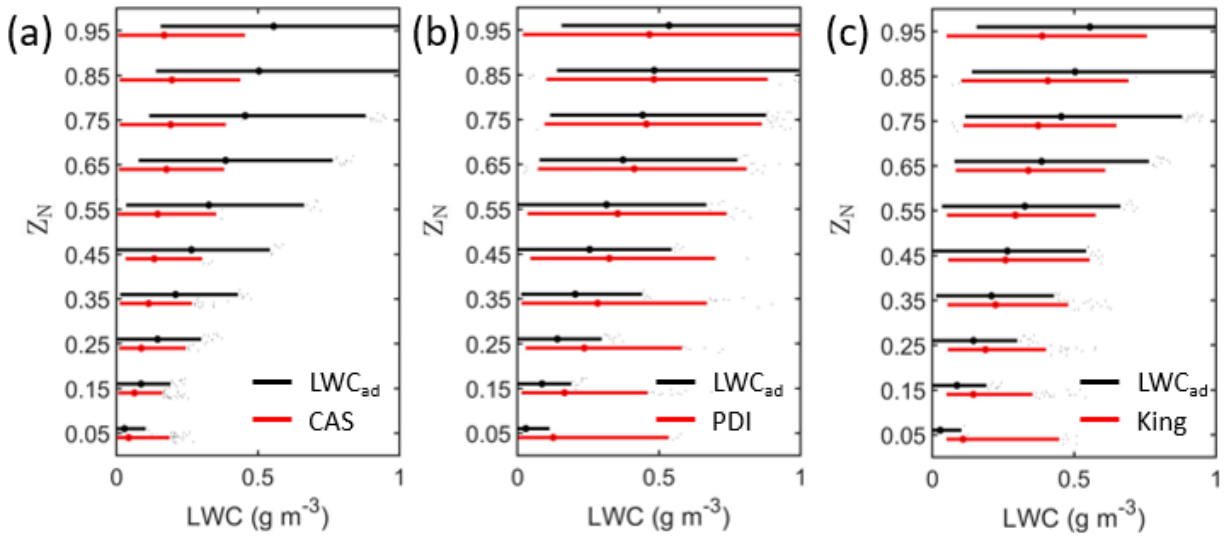
Figure 3: Boxplots representing profiles of (a) CAS LWC, (b) PDI LWC, and (c) King LWC with adiabatic LWC (LWC$_{ad}$) as function of normalized height above cloud base (Z$_N$). These data represent cloud samples from cloud profiles flown during six research flights from 2016.
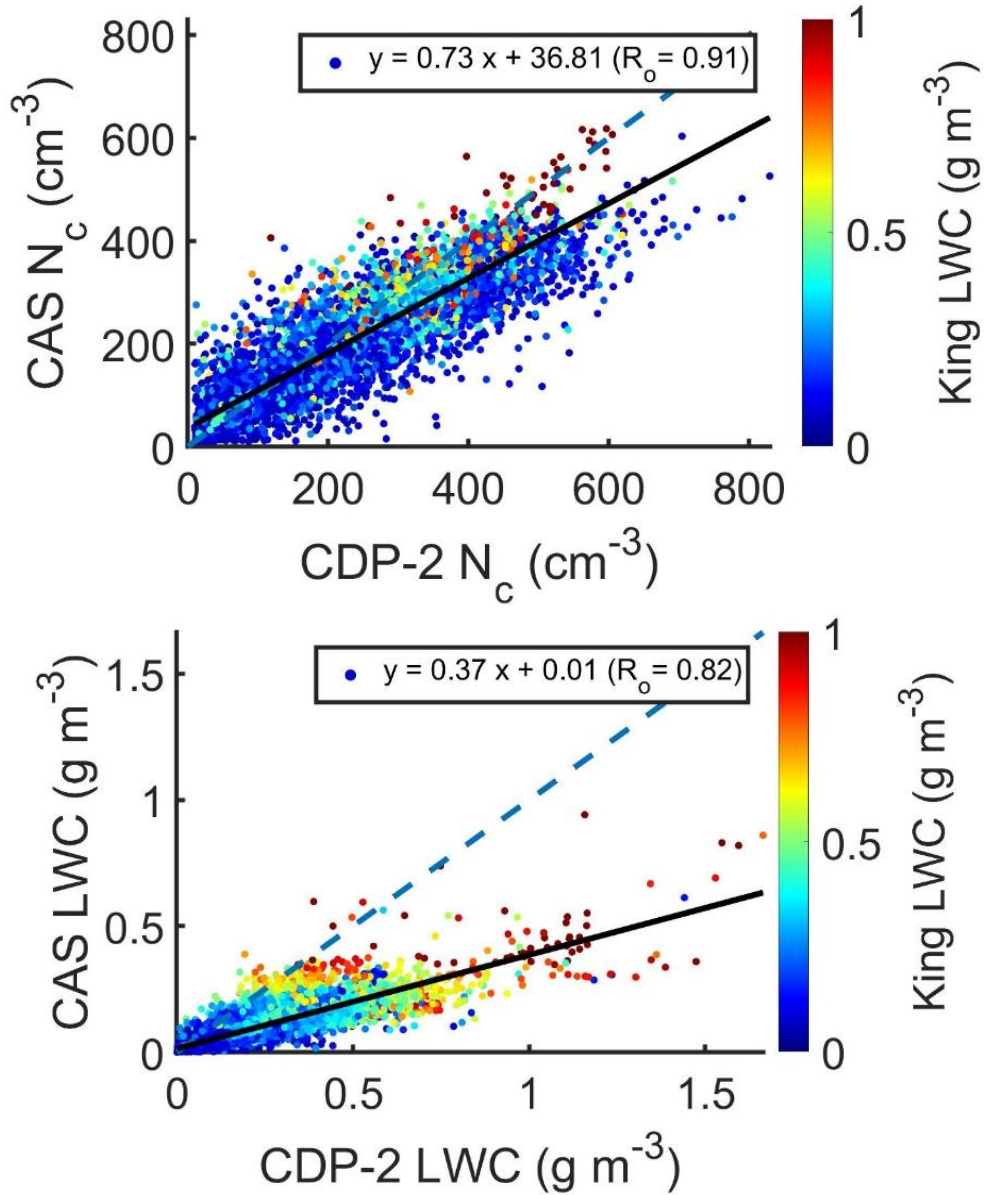
Figure 4: Scatter plots between N_c (top) and LWC (bottom) from CAS and CDP-B during 10 research flights from ORACLES 2017 (after excluding 30 and 31 August 2017). Each point represents a 1-Hz data sample colored by the King LWC.
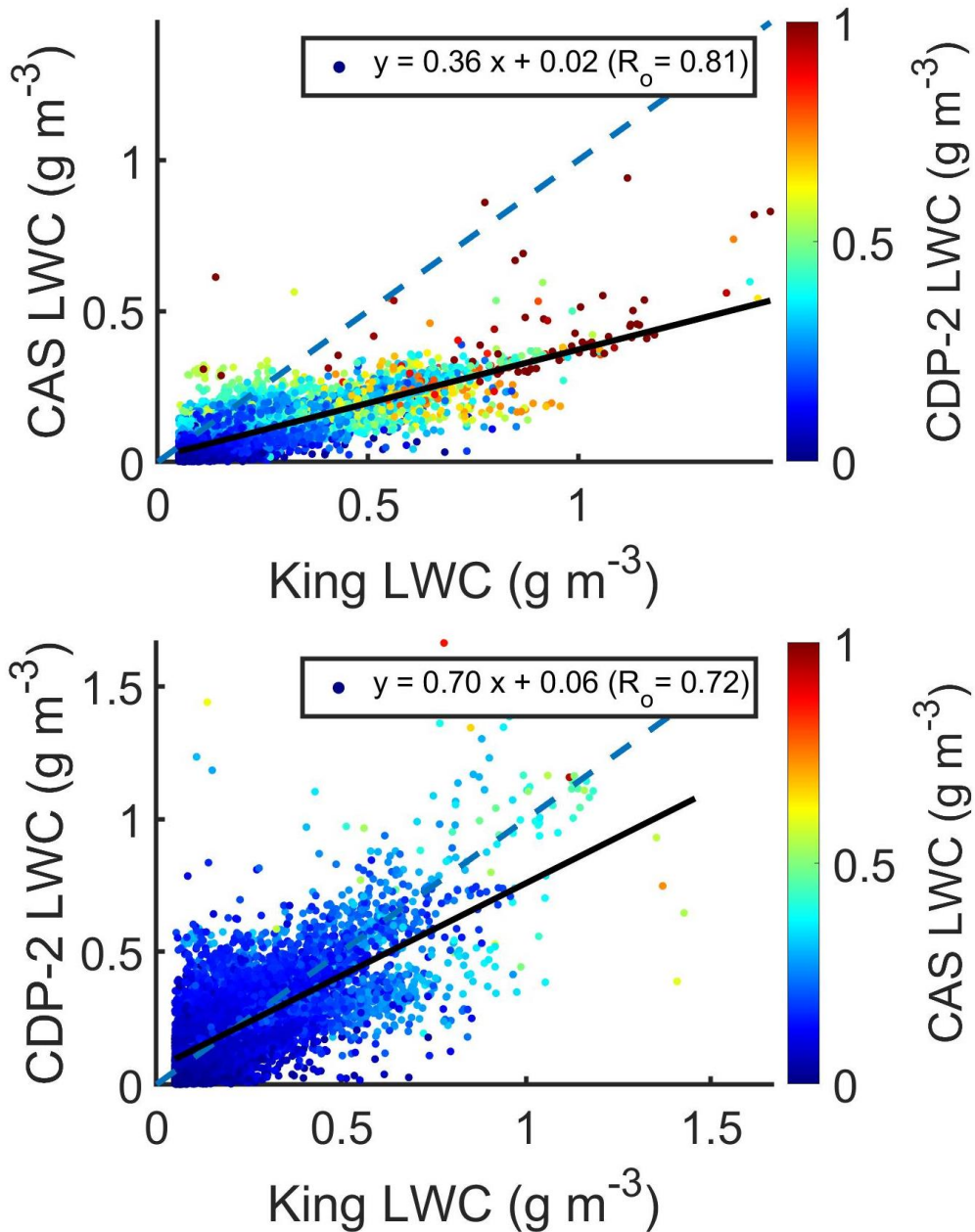
Figure 5: Scatter plots between bulk LWC with CAS LWC (top) and CDP-B LWC (bottom) for ORACLES 2017. Each point represents a 1-Hz data sample colored by CDP-B LWC (top) and CAS LWC (bottom).
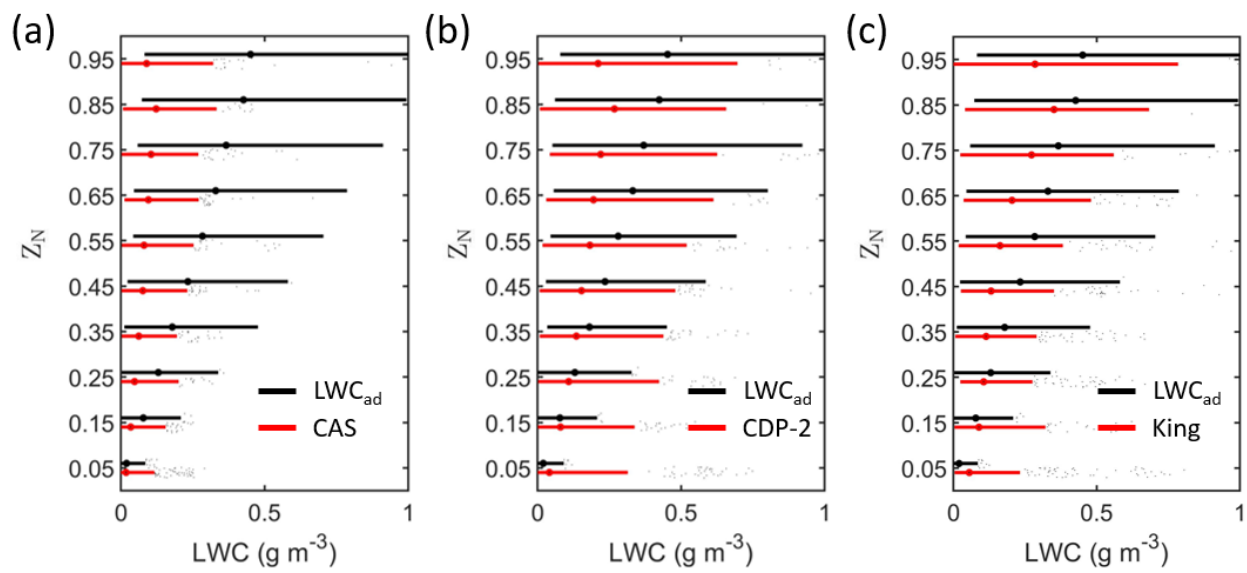
Figure 6: Boxplots representing the vertical profiles of (a) CAS LWC, (b) CDP-B LWC, and (c) King LWC with LWC_{ad} as function of Z_N. These data represent cloud samples from cloud profiles flown during seven research flights from 2017.
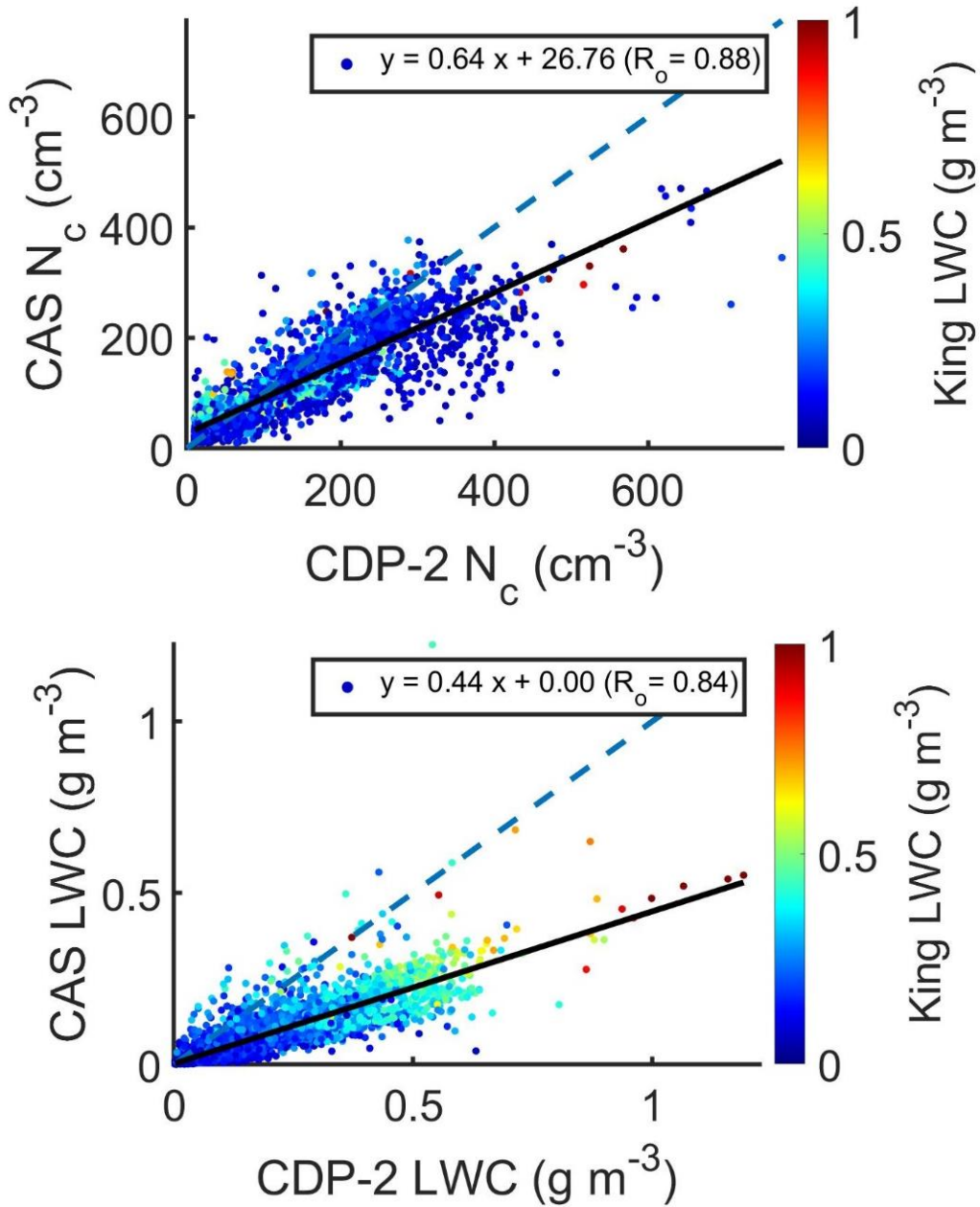
Figure 7: Scatter plots between N_c (top) and LWC (bottom) from CAS and CDP-B during the first six research flights from ORACLES 2018. Each point represents a 1-Hz data sample colored by the King LWC.
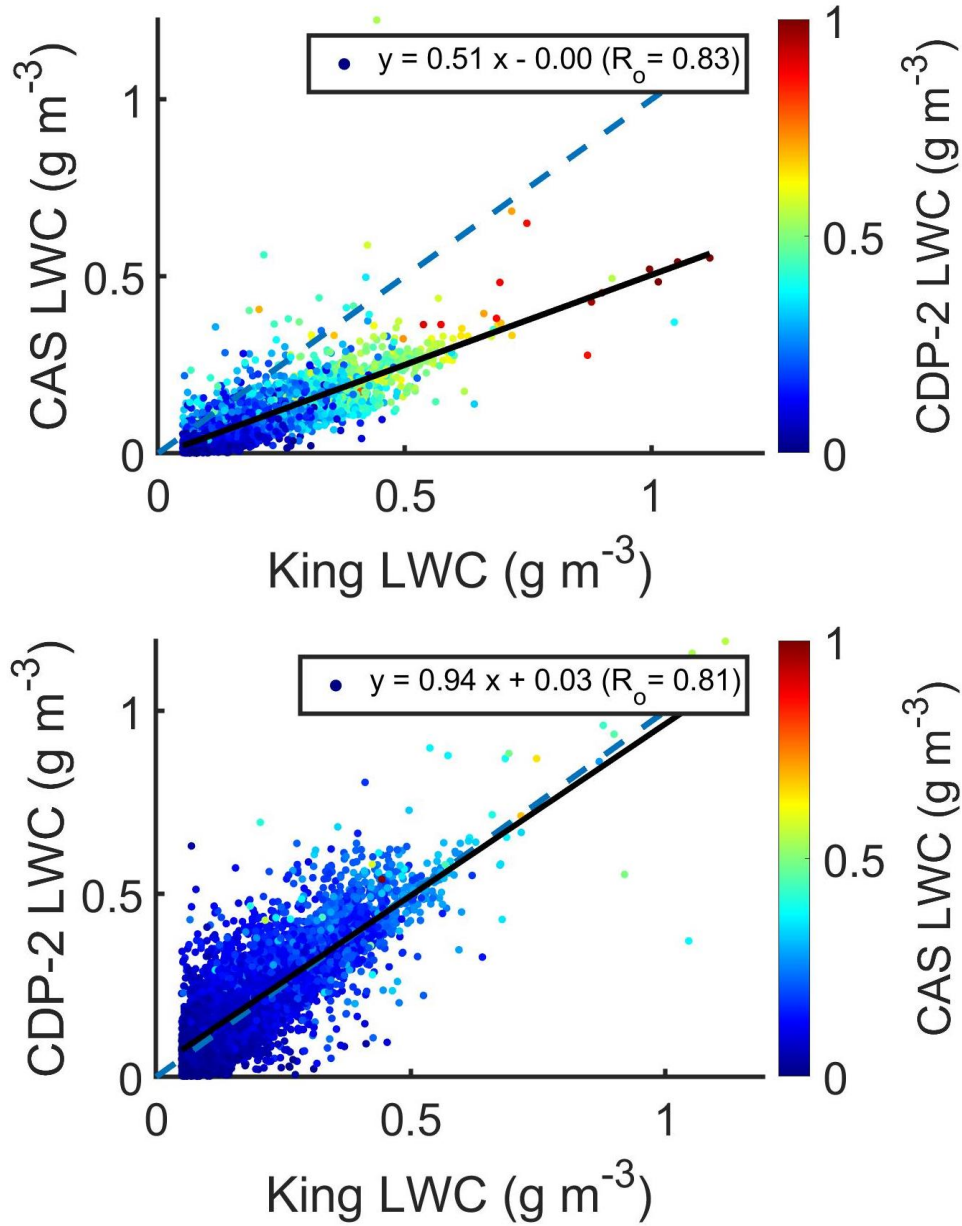
Figure 8: Scatter plots between bulk LWC with CAS LWC (top) and CDP-B LWC (bottom) for ORACLES 2018. Each point represents a 1-Hz data sample colored by CDP-B LWC (top) and CAS LWC (bottom).
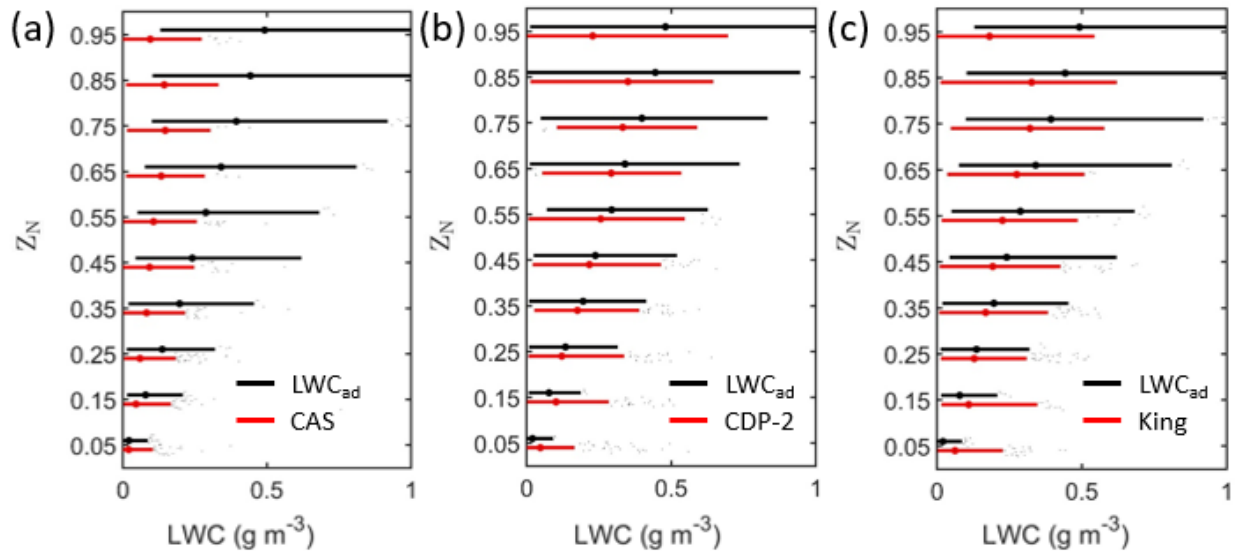
Figure 9: Boxplots representing the vertical profiles of (a) CAS LWC, (b) CDP-B LWC, and (c) King LWC with LWC_{ad} as function of Z_N. These data represent cloud samples from cloud profiles flown during the first six research flights from 2018.
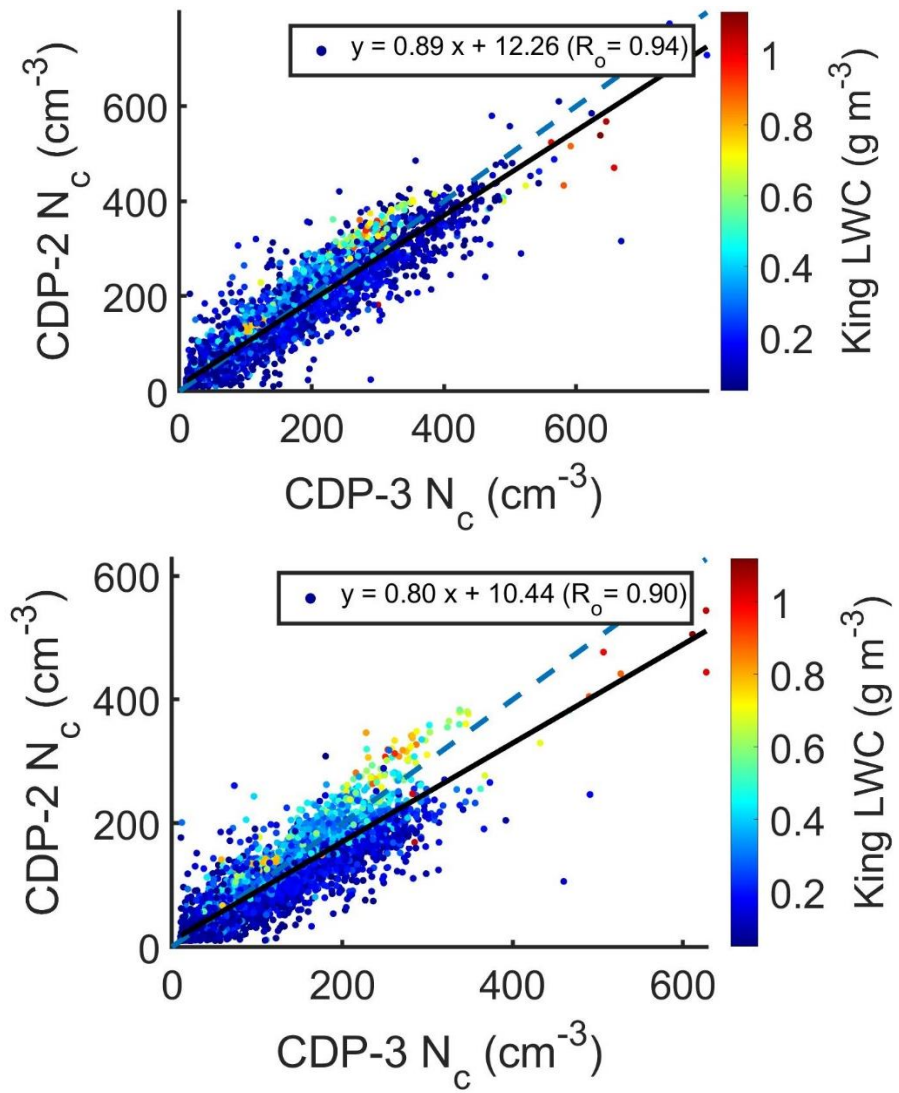
Figure 10: Scatter plots between N_c from CDP-B and CDP-C calculated from N($D > 3$ μm) (top) and N(D > 7.5 μm) (bottom) during the first seven research flights from ORACLES 2018 (before the CDP locations were switched). Each point represents a 1-Hz data sample colored by King LWC.
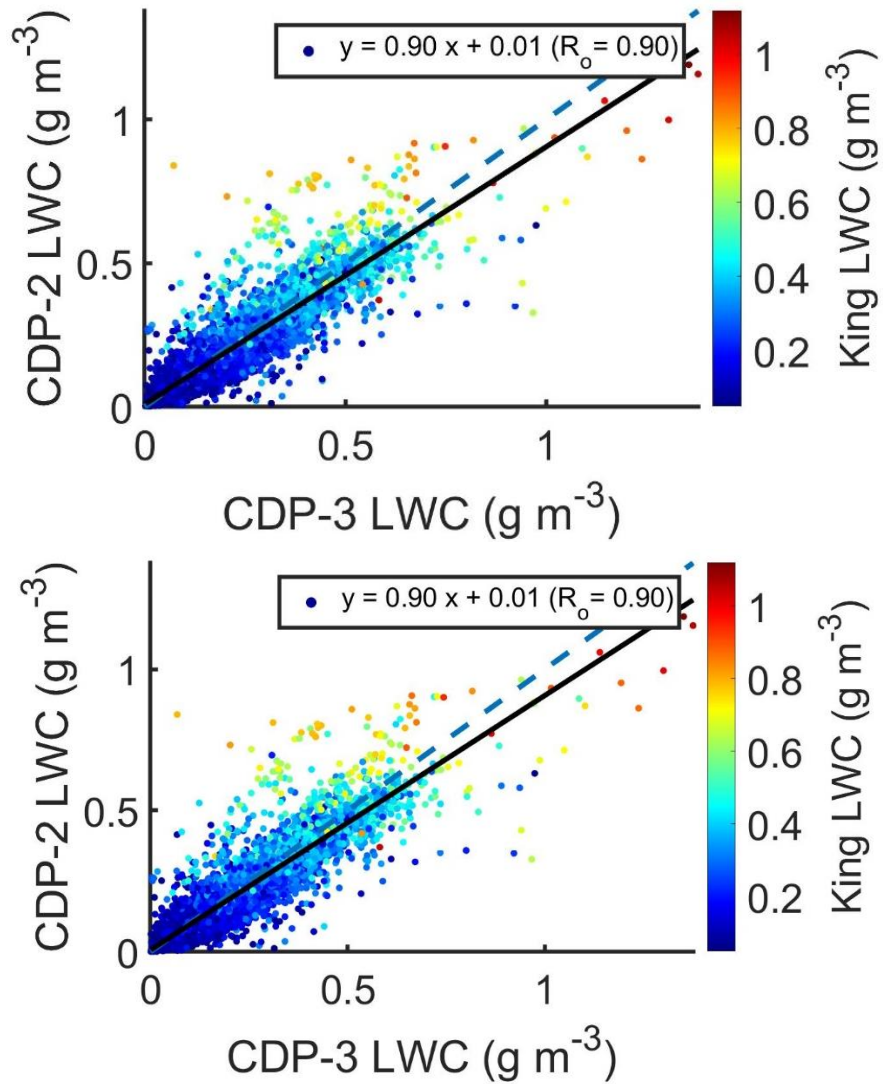
Figure 11: Scatter plots between LWC from CDP-B and CDP-C calculated from N(D > 3 μm) (top) and N(D > 7.5 μm) (bottom) during the first seven research flights from ORACLES 2018 (before the CDP locations were switched). Each point represents a 1-Hz data sample colored by the King LWC.

Figure 12: Scatter plots between bulk LWC with CDP-B LWC (top) and CDP-C LWC (bottom) for ORACLES 2018. Each point represents a 1-Hz data sample colored by CDP-C LWC (top) and CDP-B LWC (bottom).
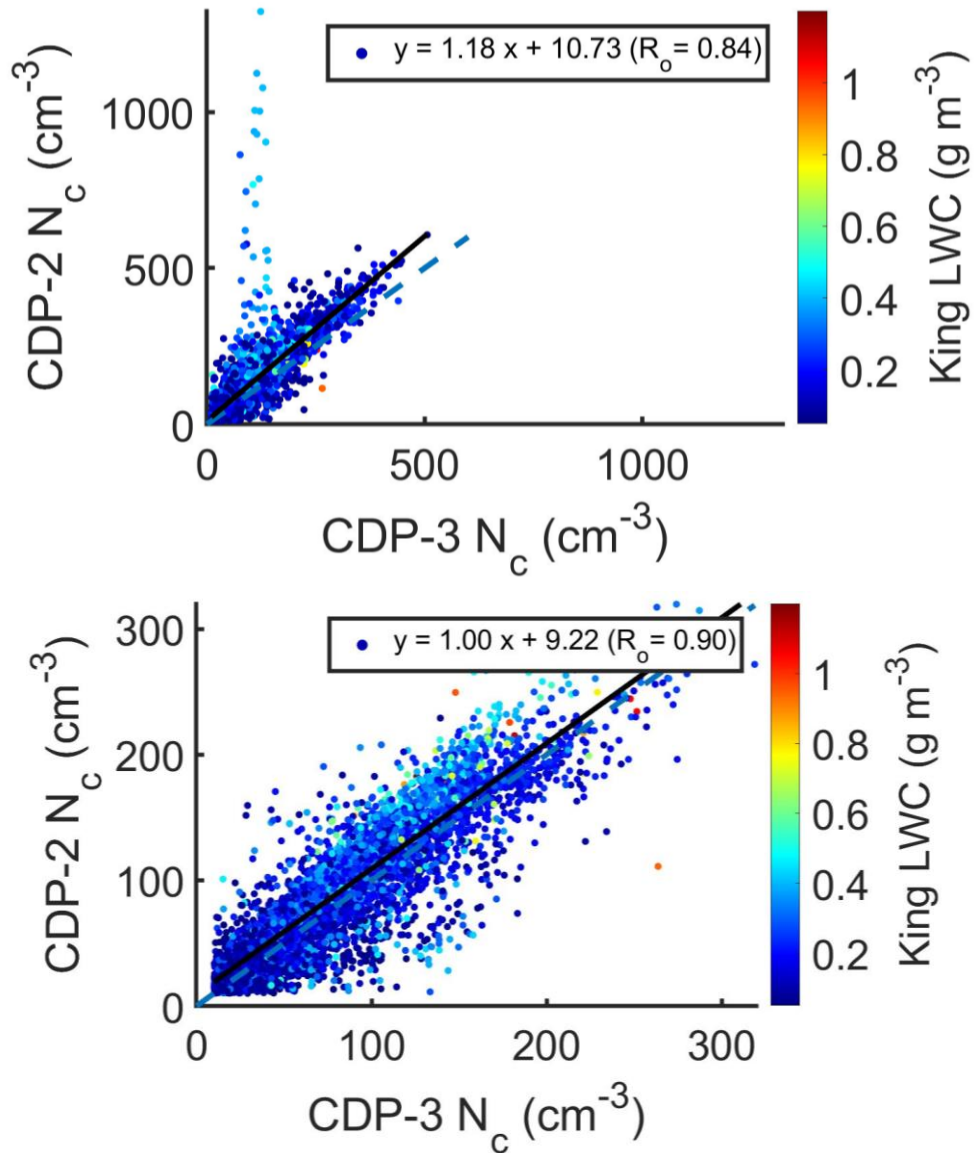
Figure 13: Scatter plots between N_c from CDP-B and CDP-C calculated from $N(D > 3\ \mu m)$ (top) and $N(D > 7.5\ \mu m)$ (bottom) during five research flights from ORACLES 2018 (after the CDP locations were switched). Each point represents a 1-Hz data sample colored by the King LWC.
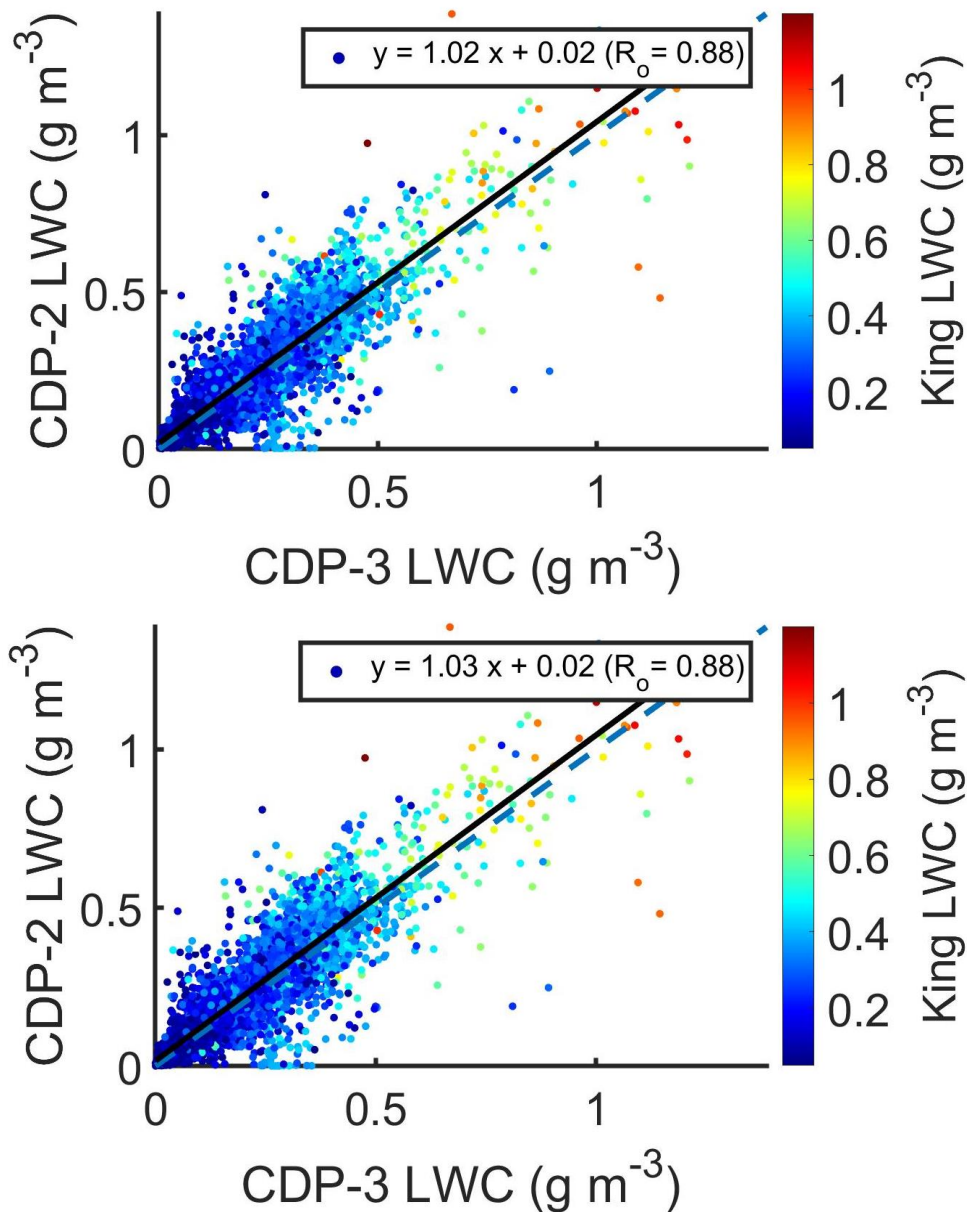
Figure 14: Scatter plots between LWC from CDP-B and CDP-C calculated from N(D > 3 μm) (top) and N(D > 7.5 μm) (bottom) during five research flights from ORACLES 2018 (after the CDP locations were switched). Each point represents a 1-Hz data sample colored by the King LWC.
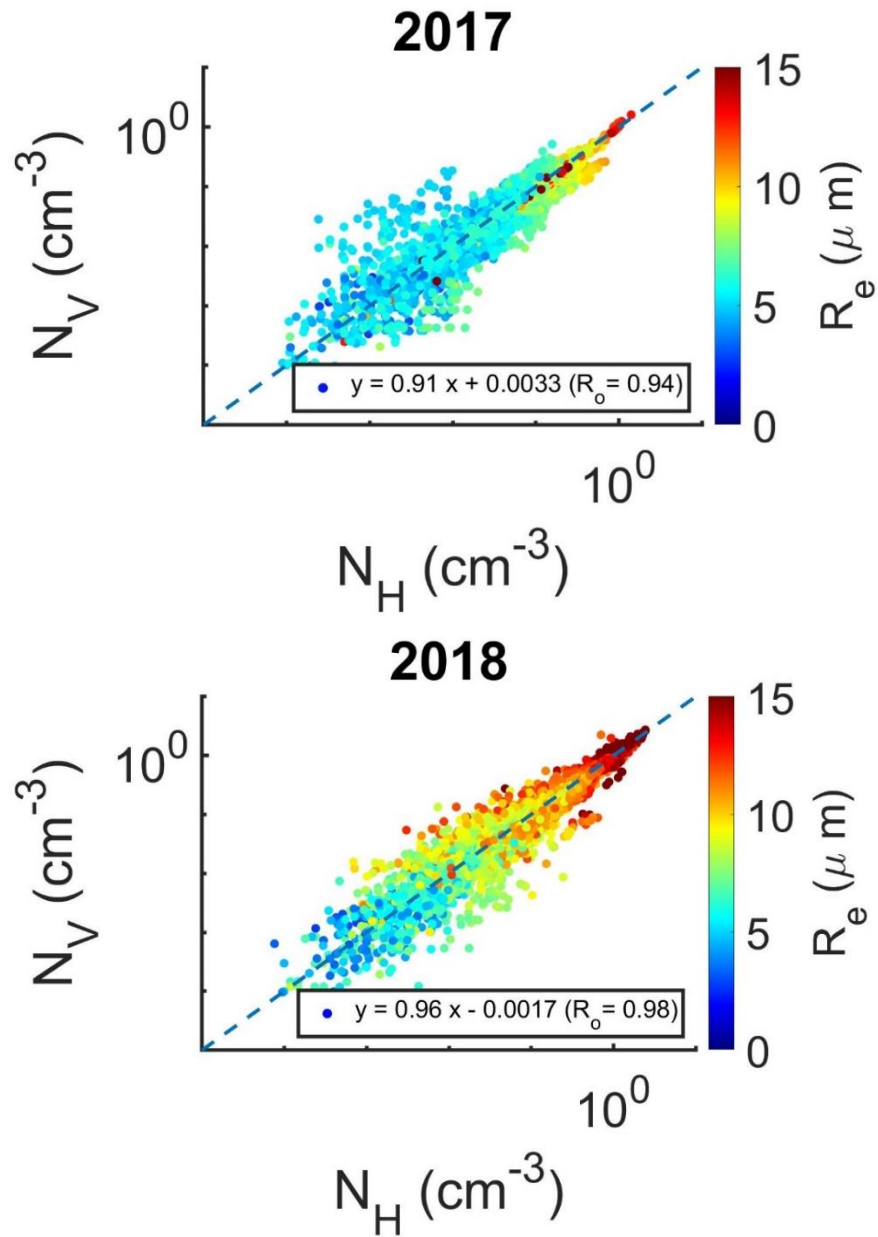
Figure 15: Scatter plots between N_H and N_V from ORACLES 2017 and 2018. Each point represents a 1-Hz data sample colored by the effective radius (R_e).
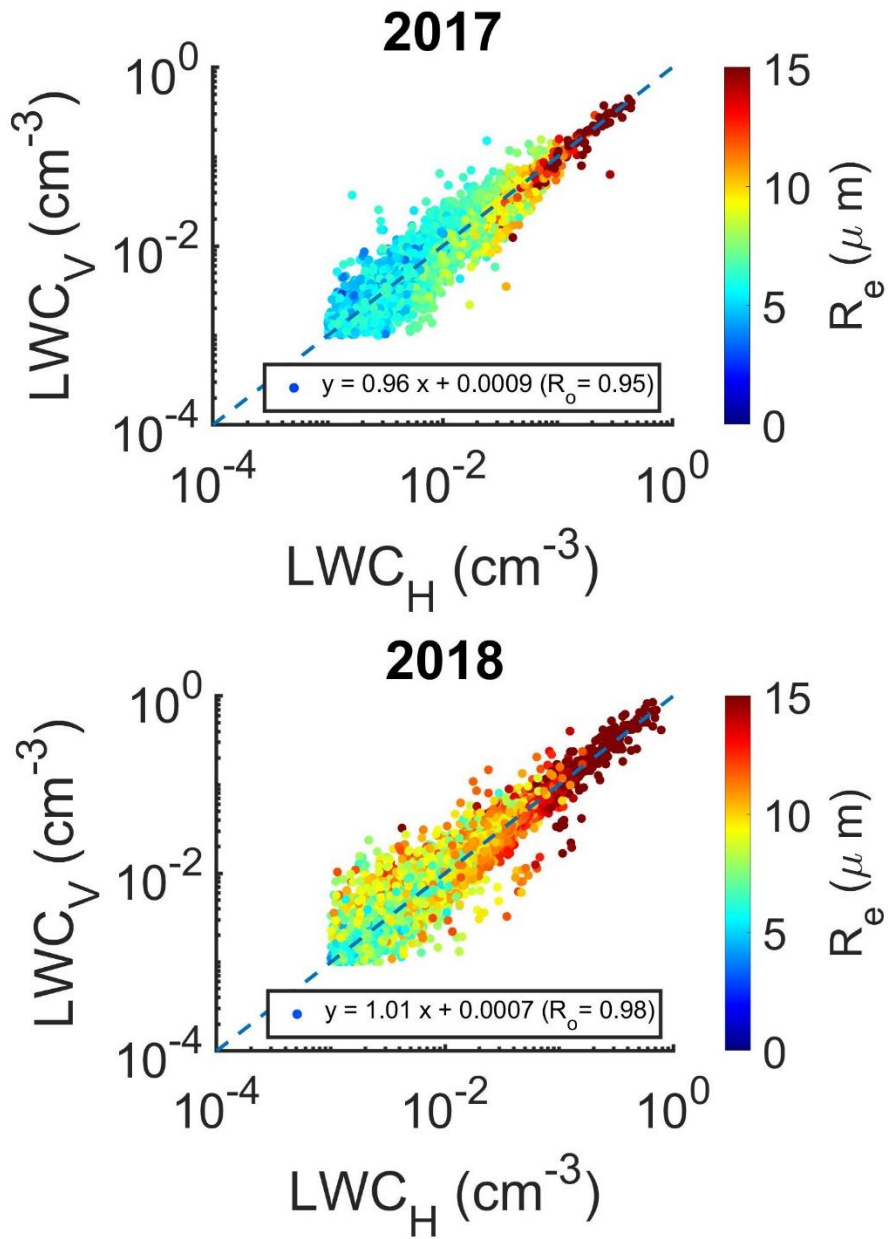
Figure 16: Same as Fig. 15 but comparing LWC_H and LWC_V.

REFERENCES:

Baumgardner, D., Jonsson, H., Dawson, W., Connor, D. O., and Newton, R.: The cloud, aerosol and precipitation spectrometer (CAPS): A new instrument for cloud investigations, Atmos. Res., 59, 59–60, 2001.

Cai, Y., Snider, J. R., and Wechsler, P.: Calibration of the passive cavity aerosol spectrometer probe for airborne determination of the size distribution, Atmos. Meas. Tech., 6, 2349-2358, https://doi.org/10.5194/amt-6-2349-2013, 2013.

Chuang, P. Y., Saw, E. W., Small, J. D., Shaw, R. A., Sipperley, C. M., Payne, G. A., and Bachalo, W.: Airborne Phase Doppler Interferometry for Cloud Microphysical Measurements, Aerosol Sci. Technol., 42, 685–703, 2008.

Delene, D. J.: Airborne Data Processing and Analysis Software Package, Earth Science Informatics, 4(1), 29-44, 2011.

Field, P., Heymsfield, A., and Bansemer, A.: Shattering and particleinterarrival times measured by optical array probes in ice clouds, J. Atmos. Ocean. Tech., 23, 1357–1371, 2006.

Gupta, S., McFarquhar, G. M., O'Brien, J. R., Delene, D. J., Poellot, M. R., Dobracki, A., Podolske, J. R., Redemann, J., LeBlanc, S. E., Segal-Rozenhaimer, M., and Pistone, K.: Impact of the variability in vertical separation between biomass burning aerosols and marine stratocumulus on cloud microphysical properties over the Southeast Atlantic, Atmos. Chem. Phys., 21, 4615–4635, https://doi.org/10.5194/acp-21-4615-2021, 2021a.

Gupta, S., McFarquhar, G. M., O'Brien, J. R., Poellot, M. R., Delene, D. J., Miller, R. M., and Small Griswold, J. D.: Precipitation Susceptibility of Marine Stratocumulus with Variable Above and Below-Cloud Aerosol Concentrations over the Southeast Atlantic, Atmos. Chem. Phys. Discuss. [preprint], https://doi.org/10.5194/acp-2021-677, in review, 2021b.

Korolev, A.: Reconstruction of the sizes of spherical particles from their shadow images. Part I: Theoretical considerations, J. Atmos. Ocean. Tech., 24, 376–389, 2007.

King, W. D., Parkin, D. A., and Handsworth, R. J.: A hot-wire liquid water device having fully calculable response characteristics, J. Appl. Meteorol., 17, 1809–1813, https://doi.org/10.1175/1520-0450(1978)017<1809:AHWLWD>2.0.CO;2, 1978.

Lance, S., Brock, C. A., Rogers, D., and Gordon, J. A.: Water droplet calibration of the Cloud Droplet Probe (CDP) and in-flight performance in liquid, ice and mixed-phase clouds during ARCPAC, Atmos. Meas. Tech., 3, 1683–1706, https://doi.org/10.5194/amt-3-1683-2010, 2010.

Lawson, R. P., Stewart, R. E., and Angus, L. J.: Observations and numerical simulations of the origin and development of very large snowflakes, J. Atmos. Sci., 55, 3209–3229, 1998.

Lawson, R. P., O'Connor, D., Zmarzly, P., Weaver, K., Baker, B. A., Mo, Q., and Jonsson, H.: The 2D-S (Stereo) probe: Design and preliminary tests of a new airborne, high-speed, high-resolution imaging probe, J. Atmos. Ocean. Tech., 23, 1462–1477, 2006.

McFarquhar, G. M., Finlon, J. A., Stechman, D. M., Wu, W., Jackson, R. C., and Freer, M.: University of Illinois/Oklahoma Optical Array Probe (OAP) Processing Software, https://doi.org/10.5281/zenodo.1285969, 2018.

O'Brien, J.R., Poellot, M., McFarquhar, G.M., Delene, D., Gupta, S., Miller, R., 2019: Cloud Droplet Probe Intercomparison from ORACLES 2018, ORACLES Science Team Meeting 2019. Miami, FL, 14-16 May 2019.

ORACLES Science Team (2020a), Moffett Field, CA, NASA Ames Earth Science Project Office (ESPO), Accessed at doi: 10.5067/Suborbital/ORACLES/P3/2016_V2

ORACLES Science Team (2020b), Moffett Field, CA, NASA Ames Earth Science Project Office (ESPO), Accessed at doi: 10.5067/Suborbital/ORACLES/P3/2017_V2

ORACLES Science Team (2020c), Moffett Field, CA, NASA Ames Earth Science Project Office (ESPO), Accessed at doi: 10.5067/Suborbital/ORACLES/P3/2018_V2

ORACLES website: https://espo.nasa.gov/oracles/content/ORACLES

Redemann, J., Wood, R., Zuidema, P., Doherty, S. J., Luna, B., LeBlanc, S. E., Diamond, M. S., Shinozuka, Y., Chang, I. Y., Ueyama, R., Pfister, L., Ryoo, J.-M., Dobracki, A. N., da Silva, A. M., Longo, K. M., Kacenelenbogen, M. S., Flynn, C. J., Pistone, K., Knox, N. M., Piketh, S. J., Haywood, J. M., Formenti, P., Mallet, M., Stier, P., Ackerman, A. S., Bauer, S. E., Fridlind, A. M., Carmichael, G. R., Saide, P. E., Ferrada, G. A., Howell, S. G., Freitag, S., Cairns, B., Holben, B. N., Knobelspiesse, K. D., Tanelli, S., L'Ecuyer, T. S., Dzambo, A. M., Sy, O. O., McFarquhar, G. M., Poellot, M. R., Gupta, S., O'Brien, J. R., Nenes, A., Kacarab, M., Wong, J. P. S., Small-Griswold, J. D., Thornhill, K. L., Noone, D., Podolske, J. R., Schmidt, K. S., Pilewskie, P., Chen, H., Cochrane, S. P., Sedlacek, A. J., Lang, T. J., Stith, E., Segal-Rozenhaimer, M., Ferrare, R. A., Burton, S. P., Hostetler, C. A., Diner, D. J., Seidel, F. C., Platnick, S. E., Myers, J. S., Meyer, K. G., Spangenberg, D. A., Maring, H., and Gao, L.: An overview of the ORACLES (ObseRvations of Aerosols above CLouds and their intEractionS) project: aerosol–cloud–radiation interactions in the southeast Atlantic basin, Atmos. Chem. Phys., 21, 1507–1563, https://doi.org/10.5194/acp-21-1507-2021, 2021.

Strapp, J. W., Leaitch, W. R., and Liu, P. S. K.: Hydrated and Dried Aerosol-Size-Distribution Measurements from the Particle Measuring Systems FSSP-300 Probe and the Deiced PCASP-100x Probe, J. Atmos. Ocean. Tech., 9, 548–555, 1992.